sustainability

MDPI

Article

Decreasing the Battery Recharge Time if Using a Fuzzy Based Power Management Loop for an Isolated Micro-Grid Farm

Habib Kraiem [1], Aymen Flah [2], Naoui Mohamed [2], Mohamed H. B. Messaoud [2], Essam A. Al-Ammar [3], Ahmed Althobaiti [4], Abdullah Alhumaidi Alotaibi [5,*], Michał Jasiński [6], Vishnu Suresh [6], Zbigniew Leonowicz [6] and Elżbieta Jasińska [7]

1 Department of Electrical Engineering, College of Engineering, Northern Border University, Arar 73222, Saudi Arabia; habib.kraiem@yahoo.fr
2 Processes, Energy, Environment and Electrical Systems (Code: LR18ES34), National Engineering School of Gabès, University of Gabès, Gabès 6072, Tunisia; aymen.flah@enig.u-gabes.tn (A.F.); mednaouiing@yahoo.com (N.M.); mohamedhaytham1996@gmail.com (M.H.B.M.)
3 Department of Electrical Engineering, College of Engineering, King Saud University, Riyadh 11421, Saudi Arabia; essam@ksu.edu.sa
4 Department of Electrical Engineering, College of Engineering, Taif University, Taif 21944, Saudi Arabia; ahmed.althobaiti@tu.edu.sa
5 Department of Science and Technology, College of Ranyah, Taif University, Taif 21944, Saudi Arabia
6 Faculty of Electrical Engineering, Wroclaw University of Science and Technology, 50-370 Wroclaw, Poland; michal.jasinski@pwr.edu.pl (M.J.); vishnu.suresh@pwr.edu.pl (V.S.); zbigniew.leonowicz@pwr.edu.pl (Z.L.)
7 Department of Operations Research and Business Intelligence, Wroclaw University of Science and Technology, 50-370 Wroclaw, Poland; elzbieta.jasinska@pwr.edu.pl
* Correspondence: a.alhumaidi@tu.edu.sa

check for updates

Citation: Kraiem, H.; Flah, A.; Mohamed, N.; Messaoud, M.H.B.; Al-Ammar, E.A.; Althobaiti, A.; Alotaibi, A.A.; Jasiński, M.; Suresh, V.; Leonowicz, Z.; et al. Decreasing the Battery Recharge Time if Using a Fuzzy Based Power Management Loop for an Isolated Micro-Grid Farm. *Sustainability* **2022**, *14*, 2870. https://doi.org/10.3390/su14052870

Academic Editor: Nicu Bizon

Received: 12 February 2022
Accepted: 26 February 2022
Published: 1 March 2022

Publisher's Note: MDPI stays neutral with regard to jurisdictional claims in published maps and institutional affiliations.

Copyright: © 2022 by the authors. Licensee MDPI, Basel, Switzerland. This article is an open access article distributed under the terms and conditions of the Creative Commons Attribution (CC BY) license (https://creativecommons.org/licenses/by/4.0/).

Abstract: An isolated micro-grid has different requirements from the traditional power grids. Several energy sources may be linked for the purpose of sharing load demand without being linked to the grid. The isolated micro-grid is made up of at least one energy generator, an energy storage system, and a load portion. Because there are several energy sources and a range of models, the power flow must be managed to ensure the safety of all hardware. Monitoring the flow of power from multiple energy sources necessitates adherence to many parameters and other requirements. As a result, the goal of this work is to identify a worthwhile solution for providing the appropriate portions with the necessary power while also obtaining the necessary energy from other sources. The approach is based on the fuzzy logic controller, which is an intelligent technology. This regulator is used in an efficient process that tries to control all of the equipment in the isolated micro-grid under investigation. The MATLAB/Simulink platform is employed for simulating this proposed system, and then, the depicted results were discussed and compared. Showing the traditional relay control, the standard PI regulator, and a neural control combination process, the achieved results prove that it is possible to reduce the battery recharge time to half; if the proposed fuzzy controller is used. Then, the established controller specifications have been used for evaluating the energy performances of the hybrid energy system under a real case situation in a specific location in the world. Consequently, the obtained results prove that this proposal power management system will be largely beneficial for such energy storage applications and an energy yield can be assured during all climatic conditions and specifications.

Keywords: wind energy; photovoltaic energy; energy storage; fuzzy logic control; converters; simulation; online control; energy management; micro-grid

1. Introduction

Advanced energy storage systems are becoming a necessity in isolated regions where no grid connection exists. An isolated farm cannot only need energy from renewable energy or a diesel generator. Electrical equipment, such as electrical tractors, electrical

fluid irrigation, and a variety of other electrical machines, are used on major agriculture farms [1–3]. According to international statistics on the usage of electrical equipment in farming, more than 1,000,000 electrical tractors will be employed until 2025 [4]. Because these farms are not connected to the power grid, they rely heavily on renewable energy sources like solar panels, wind turbines, or a mix of the two [5–7]. The decision to use one of such energy sources is influenced by many criteria, including the farm's budget, location, and the amount of power required daily [8,9]. A battery pack is often employed on these farms in addition to these energy sources, each of which has its own set of flaws and issues. This will serve as a substitute for power outages and offer electrical energy for 24 h. As a result, a hybrid energy source exists, therefore controlling the power flow is required to protect the battery pack or other devices [10].

1.1. Literat Ure State of the Art

The efficiency of the indicated multisource energy is determined first by the control techniques utilized, then by the dimensions and various blocks, such as the electrical machine for a wind energy system, the numerous types of photovoltaic (PV) panels, and their accompanying inverters [11].

According to the majority of literature evaluations, the Maximum Power Point Tracking (MPPT) approach solves the problem of power stability when external parameters such as solar radiation variation (for PV systems) or wind speed variation (for wind systems) are made [12]. Various improvements to each of these energy sources' efficiency have been proposed. The perturb and observe (P&O) approach was used as a starting point, and later intelligent techniques based on optimization algorithms, such as Particle Swarm Optimization (PSO), were discovered to be more suitable [13]. The power management problem will be eased if each energy source is controlled independently and used as the primary energy source. If a photovoltaic system is utilized, the MPPT control loop can stabilize the given voltage, regardless of the radiation factor, by adjusting the electronic chopper duty cycle. This is also true for wind energy systems, where the MPPT approach can improve the output voltage regardless of wind speed by regulating the propeller pitch angle [14]. On the other hand, when a battery pack is put for storing or solving energy, the connection between this energy storage device and all of these energy sources must be carefully evaluated to ensure that the overall system is protected from overload and battery pastime [15]. A buck-boost inverter is used to control the battery charge and discharge phases and connects the various elements, such as the wind generator, PV system, battery pack, and load. The overall system control is based on a relay control theory, according to several reviews. When the battery SOC is high, the goal is to provide the order for a discharge, and when the battery SOC is low, the aim is to be in recharging mode. As a result, a binary decision is taken in order to regulate this system [16,17].

1.2. Statement about the Paper Contribution

This research addresses the issue and proposes a new method for regulating energy flow from various sources and blocks within this isolated grid. The approach is based on a fuzzy logic controller, with the goal of monitoring the available power from each of these sources as well as the battery charge level. The control concept guarantees that the load charge receives the necessary power and that any excess energy is kept in the battery pack. As a result, the total system is correctly overseen by dynamic management of the buck and boost converters, and there is no possibility of overcharging. This method takes into account all external factors and, as a result, provides an energy storage yield when compared to the typical control architecture. The proposed control architecture was evaluated using three traditional controllers, the Standard Relay ON-OFF control, the PI controller, and a neural network combination.

After proving the benefit of the proposed control strategy and rules, the given control architecture was theatrically evaluated for a real case study, and the possible benefit of this control proposal was estimated.

1.3. Paper Organization

The paper is divided into six sections. An introduction section outlines the paper proposal and gives a rough understanding of the significance of the article. Second, the various energy sources are exposed by displaying their mathematical models in order to facilitate the construction of these blocks during the modeling phases. The control flowchart is shown and explored in the third section. Also, the fuzzy control configuration is shown, and the designed rules are cited. The fourth component is intended to display the obtained findings and statistics, which provide insight into the suggested solution's efficiency when compared to the binary control approach. Finally, this paper is brought to a close with a conclusion and offers some perspectives for the presented work.

2. The Isolated Micro-Grid Composition

The isolated micro-grid system can be composed of a variety of energy sources such as the Photovoltaic generator, the wind system, a methanation system, possibly even a hydraulic generator in such farm places. All these energy sources must be connected to serve the load part and when there is excessive production of electrical energy, an electrical storage system must appear.

2.1. Photovoltaic Generator

A photovoltaic generator is a set of solar panels that convert light energy (sunlight) into electrical energy that varies depending on the influence of light and temperature, using solar cells that are connected in series and/or parallel to each other to obtain desired characteristics such as power, voltage, and current. As shown in the diagram, the equivalent circuit of a solar photovoltaic (PV) has numerous types [18–20]. It is determined by the number of diodes connected in series. One parallel diode, shunt resistance, series resistance, a current source, and a diode are all included in the basic version. For a single diode model, the modeling step begins with expressing the output current as shown in Equation (1).as it is in [21]:

$$I_{PV} = I_{Ph} - I_D - I_P \tag{1}$$

The current of a single cell is calculated by integrating the temperature and irradiation factors:

$$I_{Ph} = [I_{sc} + K_i .(T - T_n)].\frac{G}{G_n} \tag{2}$$

Equation (3) presents the current in the path of the diode:

$$I_D = I_0\left(e^{\frac{(V_{oc})}{a.V_t}} - 1\right) \tag{3}$$

The thermal voltage of a diode is given as in Equation (4).

$$V_t = \frac{k.T.n_s}{q} \tag{4}$$

The diode saturation current I_0 depends on the temperature of the panel. I_P is the current passing through the parallel resistance of the circuit. All of these parameters may be found in Equations (5) and (6), respectively.

$$I_0 = I_{0,n}.\left(\frac{T}{T_n}\right)^3.\exp\left[\frac{q.E_g}{a.k}.\left(\frac{1}{T_n} - \frac{1}{T}\right)\right] \tag{5}$$

$$I_P = \frac{V + I_{PV}.R_s}{R_p} \tag{6}$$

Then, the expression (1), becomes as it is in Equation (7).

$$I_{PV} = [I_{sc} + K_i.(\ T - T_n\ )].\frac{G}{G_n} - I_0\left[e^{\frac{(V+I_{PV}.Rs)}{a.V_t}} - 1\right] - \frac{V + I_{PV}.R_s}{R_p} \quad (7)$$

As a result, once the number of panels in serial or parallel is determined, the whole PV system voltage and current can be stated as in Equations (8) and (9), respectively.

$$V_{PV} = N_s.\left(\frac{a.K.T}{q}\right)\ln\left\{\frac{N_p.I_{ph} - I_{pv} + N_p.I_s}{N_p.I_s}\right\} - \frac{N_s}{N_p}.\ I_{pv}.R_s \quad (8)$$

$$I_{PV} = I_{Ph}.N_p - I_0.N_P - \left[e^{\frac{(V+I_{PV}.Rs.\frac{N_s}{N_p})}{a.V_t N_s}} - 1\right] - \frac{V + I_{PV}.R_s\frac{N_s}{N_p}}{R_p.\left(\frac{N_s}{N_p}\right)} \quad (9)$$

The maximum power equals 1.5 kW that can be given by the built PV model. The model was built using the datasheet's accessible information. Table 1 illustrates the PV module's essential specifications. To develop a model of a 250 W solar photovoltaic module, a real PV module SUN EARTH SOLAR POWER TPB156x156-72-P 250 W was considered as a standard module.

Table 1. PV system parameters per PV panel.

Parameters	Values	Parameters	Values
I_{Ph}	7.9163 A	K_i	0.07 %/deg.C
I_0	1.3196×10^{-10} A	a	0.9467
I_{sc}	7.89 A	T	273 + (10, 15, 25, 30) K
V_{oc}	43.4 V	T_n	298 K
R_s	0.53082 Ω	G	(500, 750, 1000) W/m^2
R_p	159.1067 Ω	G_n	1000 W/m^2
V_{mp}	34.4 V	I_{mp}	7.27 A
K	1.38×10^{-23} J/K	E_g	1.2 eV
q	1.6×10^{-19} C	n_s	72
P_{PV}	5 kW	V_{PV}	172 V
I_{PV}	29.069 A	$N_s * N_p$	5*4

2.2. Wind Turbine

As it is known, the wind turbine system is made up of two main components. The mechanical subsystem, which describes the propeller part and the gearbox tool, which adapts the torque and speed from the two sides and converts the wind power to a mechanical power adapted to the electrical subsystem. This second subsystem is built on an electrical machine, which can be any of several different types of electrical machines [22]. At the end of this loop, a variety of converters and inverters are used to adapt the outputted voltage to the main load or charge. Figure 1 shows this loop. In this research work, the permanent magnet machine is used to build the global wind system. In the next section, the corresponding mathematical model is given and described [23].

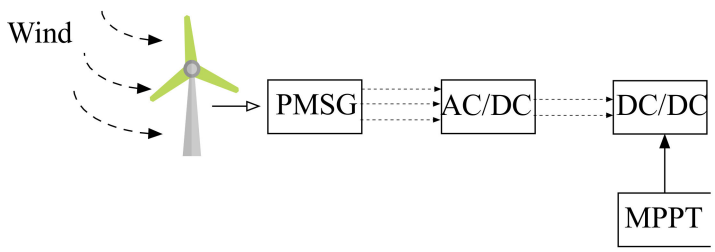


Figure 1. Wind system control loop.

2.2.1. Mechanical Subsystem

Equation (10) gives the mechanical power output of the wind turbine [24].

$$P_m = P_w.\, C_p = \frac{1}{2}.\rho.S.V_w^3.C_p(\lambda, \beta) \tag{10}$$

(C_p) represents the power coefficient of the wind turbine. It is expressed in Equation (11).

$$C_p(\lambda, \beta) = C_1.\left(\frac{C_2}{\lambda_i} - C_3.\beta - C_4\right).e^{-\frac{C_5}{\lambda_i}} + C_6.\lambda \tag{11}$$

λ_i is given by Equation (12) as:

$$\lambda_i = \frac{1}{\frac{1}{\lambda + 0.08.\beta} - \frac{0.035}{\beta^3 + 1}} \tag{12}$$

Equation (13) presents The Tip speed ratio.

$$\lambda = \frac{\mathrm{R}.\,\Omega}{V_v} \tag{13}$$

Generally, the wind turbine specification can be analyzed by the curve, which draws the evolution of the power coefficient C_p in concordance to the angle of orientation β of propellers and the specific speed of the main shaft of the propellers noted λ. Figure 2 gives this relationship. According to the law of Betz, this coefficient can reach a maximum value of 59% in theory but practically it can reach 40% for the most efficient wind turbines [25].

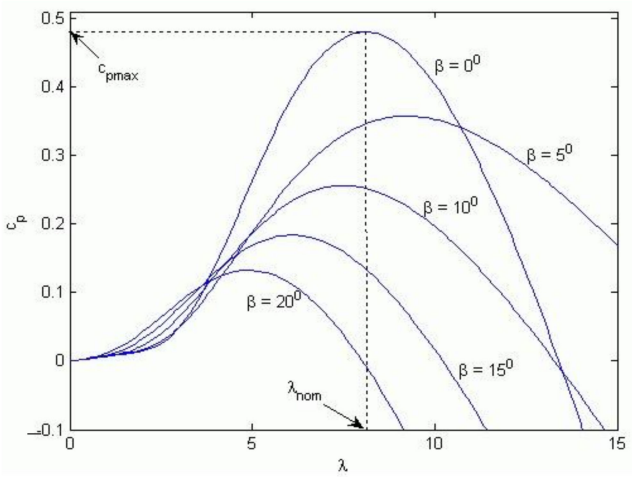


Figure 2. Wind system parameters according to the propeller orientation factor.

The mechanical angular speed of the turbine is calculated using the relationship between the electrical torque and the mechanical torque, which includes the mass of the generator and the turbine as in Equation (14).

$$J\frac{d\omega_m}{dt} = T_e - T_m - F.\omega_m \tag{14}$$

2.2.2. Electrical Subsystem

For the final output desired physical parameter, which is the electrical current, an electrical machine is used to generate the electrical power. Modeling this block is necessary for completing all the generator block equations [26].

The use of the permanent magnet synchronous generator (PMSG) is preferable for WT technology. Due to its permanent magnets, the dynamic model of the PMSG does not

depend on equations related to the rotor winding. For this, we can develop the dynamic model of the PMSG by using the equations of Voltage and flux. The voltage system of the equation noted (V_s^{abc}) and magnetic flux system of the equation noted ($Ø_s^{abc}$) can be visualized in Equations (15) and (16). All of these systems are created in a three-phase process (ABC) [27,28].

$$V_s^{abc} = r_s.i_s^{abc}.\frac{dØ_s^{abc}}{dt} \tag{15}$$

$$J\frac{d\omega_m}{dt} = T_e - T_m - F.\omega_m \tag{16}$$

The rotor reference frame can be used to characterize the PMSG's dynamic model. As a result, the voltage system of equations in the d and q axes is:

$$V_{qs} = r_s.i_{qs}.L_q.\frac{di_{qs}}{dt} + \omega_r.\ L_d.i_{ds}.Ø_m \tag{17}$$

$$V_{ds} = r_s.i_{ds} + \frac{di_{ds}}{dt} - \omega_r.L_q.i_{qs} \tag{18}$$

The electromagnetic torque is given by:

$$T_e = \left(\frac{3}{2}\right).\left(\frac{\mathrm{P}}{2}\right).\left(Ø_{\mathrm{m}}.\ \mathrm{i_{qs}} + \left(\mathrm{L_d} - \mathrm{L_q}\right).\mathrm{i_{qs}}.\ \mathrm{i_{ds}}\right) \tag{19}$$

The parameters of the wind system can be visualized in Table 2.

Table 2. Wind system parameters.

Mechanical Parameters				Electrical Parameters	
Parameter	**Value**	**Parameter**	**Value**	**Parameter**	**Value**
P_{me}	13,500 W	C_4	5	T_e	50 N.m
C_p	0.48	C_5	21	P	4
V_w	– m/s	C_6	0.0068	O_m	0.1688 web
λ	1.2	S	33.36 m^2	r_s	0.0918 Ω
Ω	300 tr/min	ρ	1.292 Kg/m	ω_r	314.159 tr/min
R	3 m	J	148.5 Kg.m^2		
β	0 deg	F	1.4 N.m.s/rad		
C_1	0.5176	ω_m	31.41 rad/s		
C_2	116	T_m	45 N.m		
C_3	0.4				

2.3. Lithium Battery Pack

The main component inside this energy loop is based on the electric energy accumulator, which is based on the lithium battery version. For assuring the needed simulation and studying correctly the comportment of this system, a mathematical battery model is required to characterize the electrical characteristics. The given mathematical model is based on a Second-Order RC Equivalent Circuit Model (ECM) to describe the external electrical performance of the battery, as shown in Figure 3. The ECM consists of an open circuit voltage source (OCV), an internal ohmic resistance R_0, and two parallel RC arrays. Resistance R_1 and capacity C_1 are used to simulate the reactivity distribution to capture the local characteristics of the electrolyte. The charge transfer resistor R_2 and the double-layer electrical capacity C_2, are used to represent the interface impedance of the battery [29–32].

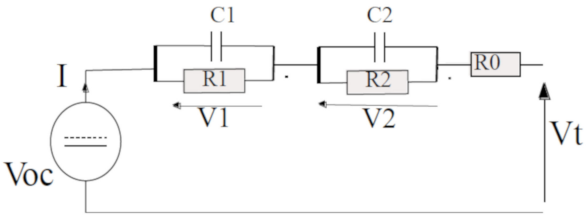


Figure 3. Battery pack: equivalent electrical diagram.

The differential equations of the ECM are exposed in Equations (20)–(22).

$$\frac{dV_1}{dt} = -\frac{V_1}{R_1.C_1} + \frac{I}{C_1} \tag{20}$$

$$\frac{dV_2}{dt} = -\frac{V_2}{R_2.C_2} + \frac{I}{C_2} \tag{21}$$

$$V_t = V_{oc}[SOC(t)] - V_1 - V_2 - I.R_0 \tag{22}$$

I is the current, R_0 represents the Ohmic resistance of the storage device, V_1 and V_2 denote the polarization voltage over $R_1.C_1$ and $R_2.C_2$, respectively V_t is the terminal voltage, V_{oc} represents the open-circuit voltage (OCV), which is a function of SOC.

The SOC value can be expressed as in Equation (23), where Q_n is the battery rated capacity [33].

$$SOC(t_1) = SOC(t_0) - \int_0^{t_1} \frac{I(t)dt}{Q_n} \tag{23}$$

The battery rated capacity depends on the effect of the capacity fading. The remaining battery capacity available is expressed in Equation (24) [34].

$$Q_n = 3600.Q_{init}.CCF \tag{24}$$

where CCF represents the Capacity correction factor and Q_{init} is the Initial battery capacity [Ah]. From the other side, the functioning of the battery system can be summarized by the following Equations (25) and (26).

$$E_{ch}(t) = E_{bat}(t-1) + (E_{HES}(t) - E_L(t)).\eta_{bat} \tag{25}$$

$$E_{dis}(t) = E_{bat}(t-1) - (E_L(t) - E_{HES}(t)) \tag{26}$$

where E_{ch} is the battery power in the charging, E_{dis} is the battery power in the discharging, η_{bat} is the battery efficiency (%), E_L is the load demand, and E_{HES} is the power delivered from the energy system (W). Figure 4 shows the discharge characteristic example of the used battery. Table 3 shows the key specification of the considered battery.

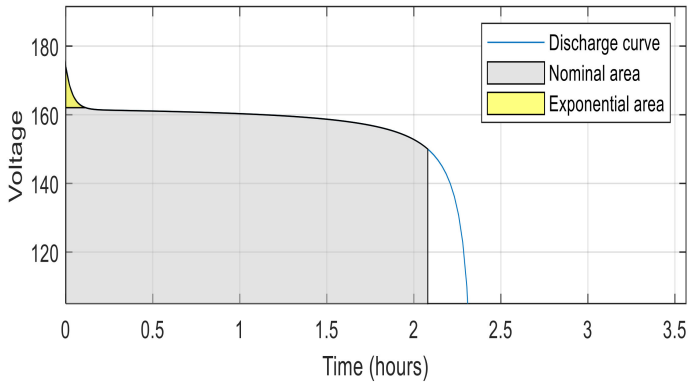


Figure 4. *Cont.*

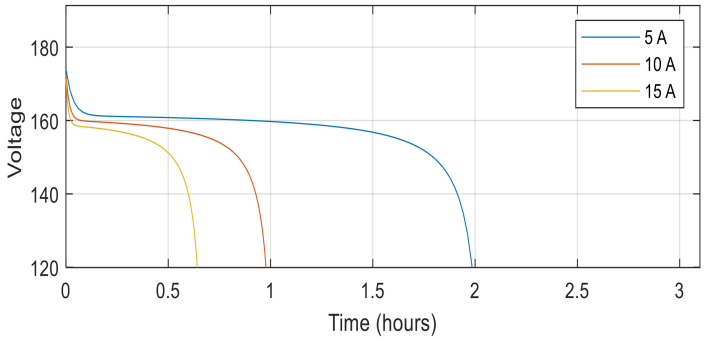


Figure 4. Discharge specification of the used battery.

Table 3. Battery system parameters.

Parameter	Value
P_n	1500 Wh
V_n	150 V
Q_n	10 Ah
R_0	0.15 Ω

2.4. Converters

Basically, numerous inverters must be used for having a DC flow from the major energy sources. A three-phase static converter based on a diode bridge rectifier (not controlled) is used to convert the alternating type (AC) electrical energy produced by the wind turbine into continuous type electrical energy (DC), connected directly by a boost converter (DC/DC) to reach the MPPT [35,36]. This last converter has the same objective for the photovoltaic system. On the other hand, a buck-boost converter (DC/DC) is installed to control the charge and discharge of the battery pack.

Based on these specific works, cited as [37,38], related to the electronic converters, it is easy to express the input and output voltage of the boost converter as in Equation (27). V_{int} is the input voltage, V_{out} is the output voltage, D is duty cycling.

$$V_{int} = \frac{V_{out}}{1 - D} \tag{27}$$

The buck-boost converter has two operation modes. It depends on the position of the Isolate Gate Bipolar Transistor (IGBT), which can be found inside. Supposing that these two switches have the nomination of K_{10} and K_{11}. The relationship between these two parameters can be expressed in Equation (28).

$$K_{11} = 1 - K_{10} \tag{28}$$

As this chopper will be connected to a battery pack from one side and a DC bus line from the other side, V_{bat} denotes the battery voltage side and V_{dc} denotes the DC bus voltage side. So, the relationship between the two voltages can be expressed as in Equation (29) and the output current can be formulated as in Equation (30).

$$L_{bat}.\frac{di_{bat}}{dt} + r_{bat}.i_{bat} = V_{bat} - V_{dc}.(1 - K_{10}) \tag{29}$$

$$I_{out} = I_{bat}.(1 - K_{10}) \tag{30}$$

3. Loop of Power Management

Because the micro-grid system is made up of a range of energy sources whose energetic performance is affected by external factors such as the weather and the location of the

sun, maximum power can be achieved only if the chopper for both systems is managed using the MPPT approach. There are several methods for the control of the MPPT, such as the P&O, the Incremental Counter, and Particle Swarm Optimization. Each of them has some specifications and based on these works, which give a priority for the PSO method, this solution was used for controlling the PV and wind choppers. From the other side, a principal controller placed between all of these sources and load parts for supervising the energy flow from the different positions is mandatory and necessary. This step is carried out using a fuzzy logic controller, as stated in the paper's purpose. The overall control loop's concept may be observed in Figure 5, which depicts the principal control loop and shows the energy flow diagram clearly.

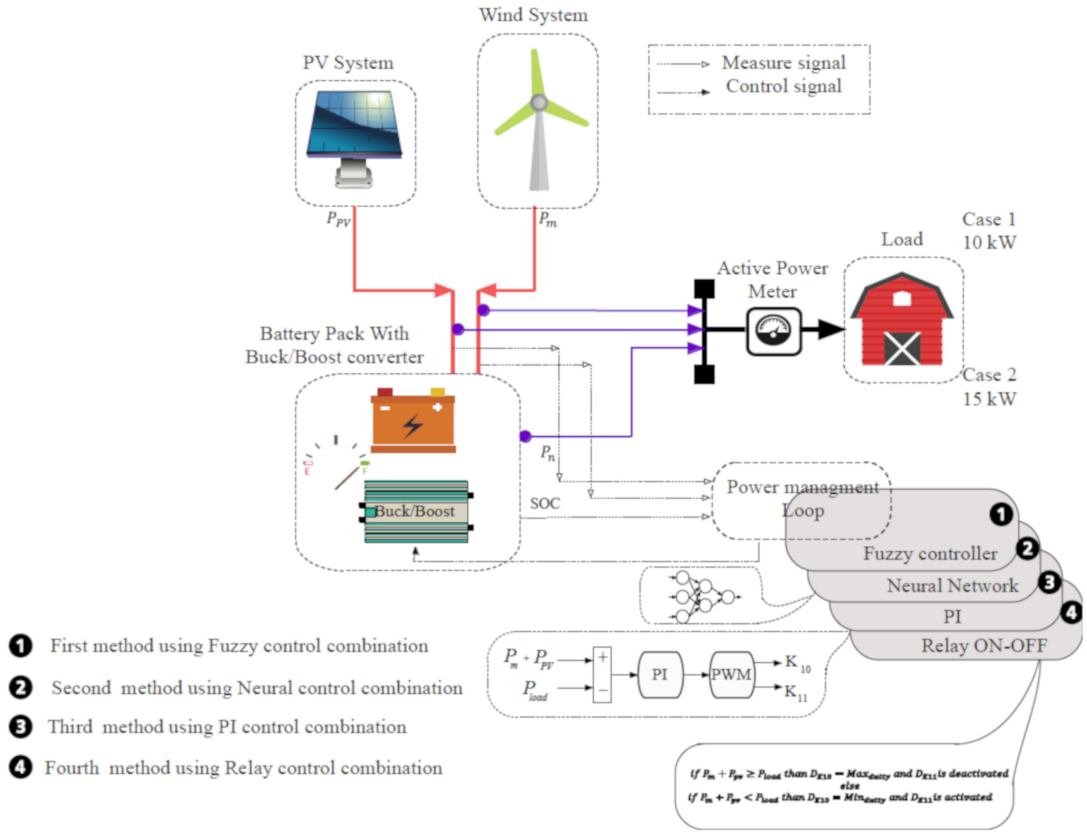


Figure 5. Micro-grid control flowchart: Four control combinations.

The idea is to continue feeding the load part from the wind system and the PV solar panels. If there is any excess energy, it is time to store the energy in the battery pack. This is true whenever the PV and the wind system can provide the required power, else it is time for the battery to be used. For other situations where no load charge is connected, the battery will be totally charged using the given power from the two sources. The power management control loop, which is based on fuzzy logic controllers and controls, the charging and discharging phases of the battery include four input signals, as shown in Figure 5. This is accomplished by determining the duty cycle of each pulse width modulator signal used to drive the buck-boost inverter.

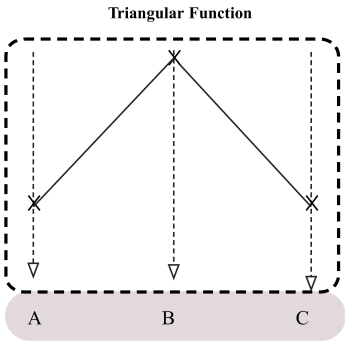
3.1. Fuzzy Controller Configuration

As is well known, there are three procedures that must be followed in order to configure the fuzzy controller. Table 4 shows how the fuzzification step was resolved. The triangle activation form is used to determine the linguistic equivalence of each input signal. Referring to Table 4, three states define each variable as the State of Charge (SOC), the given wind power denoted by P_m and the photovoltaic given power denoted by P_{PV}. As

the triangular function is used for defining each state, three points A, B, and C define the triangular points, like the right, center, and left points, respectively. For example, the first state of the SOC, denoted as small, has 100% equivalence at 0.25 ratio and 0% if it is 0 or 0.55. However, it will be 100% equivalent to the medium level at that point.

Table 4. Fuzzification phase for input signals.

Input Variable	Fuzzy Equivalence	A	B	C
SOC	Small	0	0.25	0.55
	Medium	0.25	0.5	0.75
	Big	0.5	0.75	1
P_m	Small	0	0.2	0.5
	Medium	0.2	0.5	0.8
	Big	0.5	0.8	1
P_{PV}	Small	0	0.2	0.4
	Medium	0.2	0.6	0.8
	Big	0.6	0.8	1



The active load power was meant to be consistent throughout the rest of this project, and it was attempted to lessen the complexity of the rules configuration (15 kW). As a result, only three input signals will be established for the fuzzy controller to be built.

Before being given the rules that will regulate the whole system, a defuzzification stage must be configured in addition to the fuzzification phase. The fuzzy controller sends out the control signal. It has two output data points. Each one contains the required duty cycle for controlling the buck-boost converter's related component. The comparable duty cycle factors for each of the output signals are listed in Table 5 according to their linguistic designation. Similar to the input vectors, each output vector, which defines the corresponding duty cycle of each of the IGBT components into the buck-boost converter, is divided into three states. Little, medium, and high are those states. The triangular function is the used activation model and the three limit points of the triangular form for each of these inputs and states are denoted A, B, and C.

Table 5. Defuzzification phase for output signals (duty cycle).

Output Vector	Fuzzy Equivalence	A	B	C
Out1/K_{10}	Little	0	0.1	0.15
	Medium	0.12	0.3	0.45
	High	0.45	0.75	1.0
Out2/K_{11}	Little	0	0.25	0.5
	Medium	0.2	0.5	0.8
	High	0.5	0.75	1

The corresponding rules that will manage the different input and output signals are summarized in Table 6 and Figure 6, which were concluded after several configuration tests to have satisfactory performance.

Table 6. Different rules configuration.

Rules	Input Vector			Out1/K_{10}	Out2/K_{11}
	SOC	P_m	P_{PV}		
1	Small	Big	Small	High	Little
2	Small	Big	Medium	High	Little
3	Small	Big	Big	Medium	medium
4	Small	Medium	Small	High	Little
5	Small	Medium	Medium	medium	Little
6	Small	Medium	Big	medium	Little
7	Small	Small	Small	medium	Medium
8	Small	Small	Medium	medium	Medium
9	Small	Small	Big	medium	Little
10	Medium	Big	Small	High	Little
11	Medium	Big	Medium	medium	Medium
12	Medium	Big	Big	medium	Medium
13	Medium	Medium	Small	medium	High
14	Medium	Medium	Medium	medium	High
15	Medium	Medium	Big	Little	Medium
16	Medium	Small	Small	medium	Medium
17	Medium	Small	Medium	Little	High
18	Medium	Small	Big	Little	Little
19	Big	Big	Small	medium	High
20	Big	Big	Medium	little	High
21	Big	Big	Big	little	High
22	Big	Medium	Small	medium	Medium
23	Big	Medium	Medium	little	Medium
24	Big	Medium	Big	little	High
25	Big	Small	Small	medium	High
26	Big	Small	Medium	little	High
27	Big	Small	Big	little	High

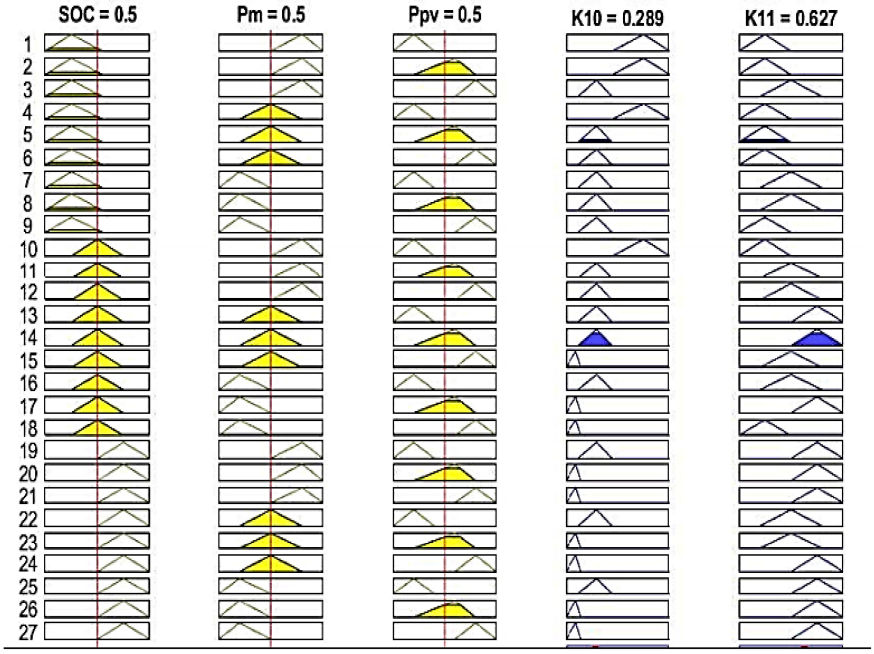


Figure 6. The 27 different rules of the fuzzy power management controller.

3.2. The Neural Network Control Combination

Similar to the previously used combination inside the fuzzy controller; three kinds of parameters were used as inputs for the neural network regulator. In this part, the neural network regulator was implemented for organizing the energy flow from the sources to the

load and the battery pack. The same inputs were used in order to make a real comparison between the two controllers and power management strategies. The neural network controller has these specifications: The learning phase was applied using a database of 5000 points for each of these inputs and outputs. There was a three-layer block for the overall architecture of this controller. The sigmoid activation function was implemented in each cell. The internal architecture was as follows: three input layers in the first stage, two cells in the middle layer, and one cell in the last layer. The training epoch number was 500. The similarity value was evaluated to be 98%. It is important to mention that the database was obtained after several variations on the solar radiation, wind speed, and battery initial SOC. The corresponding control loop can be visualized in Figure 5.

3.3. The Relay ON_OFF Control Loop

The relay control loop is the standard control process. It is the most simple control method as the decision by connecting or disconnecting the battery to the main energy source depends on the previously fixed threshold. Only a matrix of relays manages the movement of current from one side to another. In this combination, the used rules are fixed as mentioned in these two codes:

$$\begin{array}{l} if\ P_m + P_{pv} \geq P_{load}\ than\ D_{K10} = Max_{dutty}\ and\ D_{K11} is\ deactivated \\ else \\ if\ P_m + P_{pv} < P_{load}\ than\ D_{K10} = Min_{dutty}\ and\ D_{K11} is\ activated \end{array}$$

3.4. The PI Control Loop

The PI control loop is based on the comparison between the needed power from the load and the produced power from the two energy sources—the wind system and the PV panels. The duty cycle will be the output signal from the PI controller and after placing a PWM block, the corresponding signals that attack the boost and the buck converters will be delivered. It is important to mention that the PI parameters were chosen by trial and error. The corresponding scheme of the used control loop is mentioned in Figure 5 and this control method was tested only for a fixed load case.

3.5. The Simulation Results

The simulation results that demonstrate the efficiency of the power management system are disclosed and analyzed in this section. To begin, the simulation parameters were set according to the previously mentioned Tables 1 and 2 in the same way as the PV and wind systems specifications were set. The starting level of charge of the battery was set to 100%, and the load section was put to the test in two separate scenarios—a case of 10 kW and a second situation case for a larger active power equal to 15 kW.

To validate the performance of the proposed fuzzy energy management flowchart, different climatic situations are exposed and evaluated. Also, the performance of the proposed control loop was compared with the three cited controllers as mentioned before.

For all the four control methods, three daily comportments were applied: the first situation simulates the night comportment, where only the wind system can feed the battery and the load with the necessary power.

The second case is related to the daily comportment where the day can be a light day where no winds exist and then only the PV system can contribute to the micro-grid with active power.

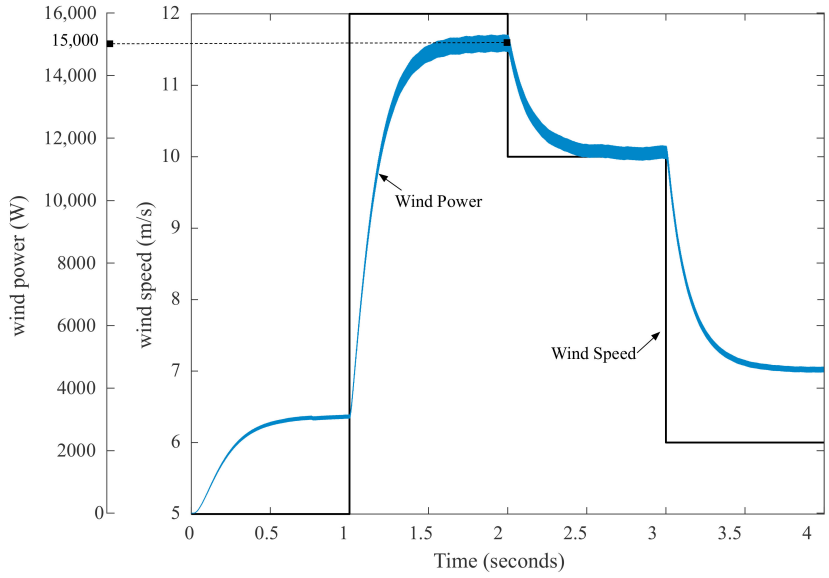
The third scenario represents the behavior of a day with a strong breeze and a brief burst of bright sunshine.

As a result, this simulation section depicts the behavior of the suggested energy management tool and compares it to a traditional control approach based on relay controllers, the PI control loop, and the neural network control loop. The objective is to demonstrate that with the proposed approach (fuzzy control loop) an energetic yield will be assured when desiring to add an energy storage system to this micro-grid and how the battery will

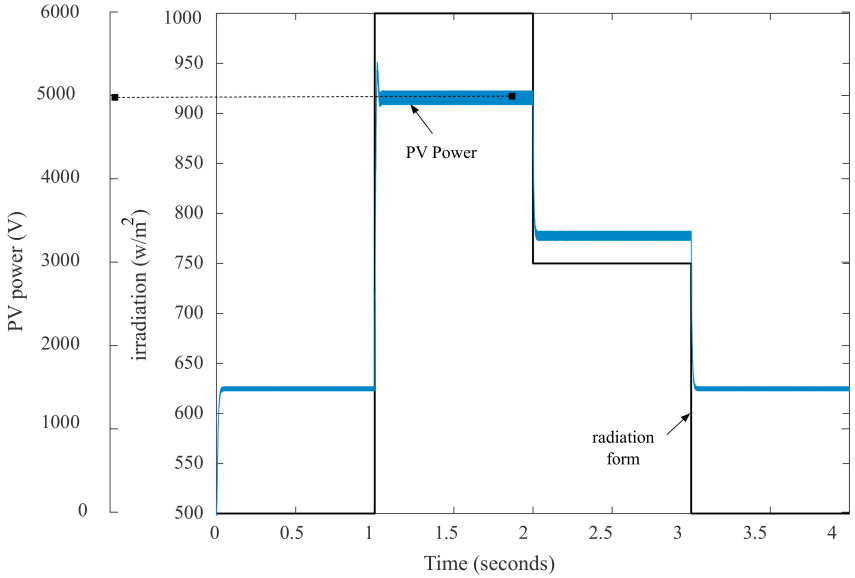
be charged or be discharged. So, the gain of energy in the battery pack will be the result of this comparison between the fuzzy control solution and the other control loops.

Case of a Stationary Load

With four seconds as a simulation time, Figure 7a,b depicts the comportment of the wind power form and the supplied photovoltaic generator form. The wind power shape is also obtained under four different wind speeds. The wind speed is 3 m/s from 0 to 1 s, and the specified power is 3 kW. The wind speed climbs to 12 m/s in 1 to 2 s, and the generated power reaches 15 kW. Then, the wind speed decreases again with two steps of four touching 5 kW at 6m/s of wind speed at the end of the simulation time.



(a) Wind power for different wind speed



(b) PV power for different solar radiation form

Figure 7. The given wind and solar radiation forms for generating wind power and solar power.

In addition, the photovoltaic power was shown under four different irradiation conditions. From 0 to 1 s, the irradiation factor is 500 and then the irradiation value increases to 1000. Correspondingly, the obtained PV power is 1.5 kW and then moves to 5 kW. Then, the obtained power decreases more as the solar radiation form decreases.

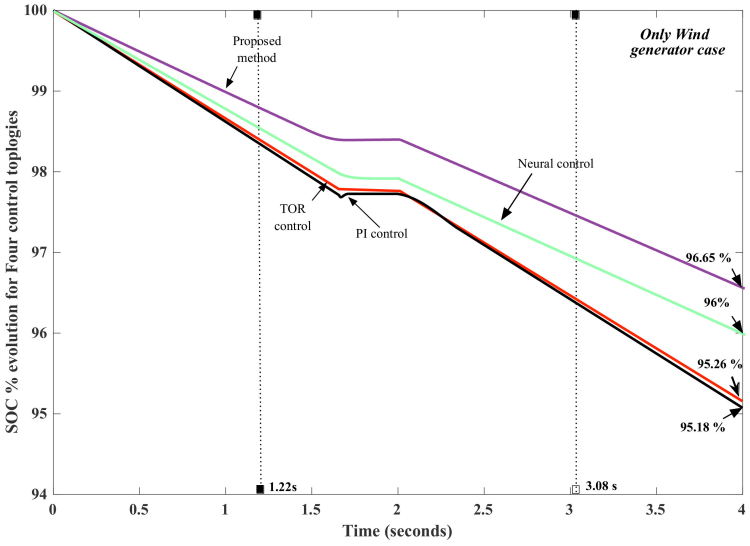
Remark 1. *The obtained PV and wind power results are based on the PSO-MPPT technique that was used for generating and stabilizing the maximum output energy from these renewable energy sources.*

This studied case has supposed that the load part will rest constantly during the simulation time and be equal to 15 kW per hour. The obtained statistics, illustrated in Table 7, give an approximation of the contribution of the PV and wind systems and evaluate what kind of energy will be available. As mentioned in Table 7, 10,500 W is needed as additional power for the first simulation second and 8500 W is the needed power in the fourth simulation second. However, extra power exists from the first to the third simulation second.

Table 7. The Given power by the PV and Wind systems for the first studied case (a load of 15 kW).

Time (s)	Wind Power (Watt)	PV Power (Watt)	Total (watt)	Extra Power(watt)	Needed Power (watt)
0 to 1	3000	1500	4500	-	10,500
1 to 2	15,000	5000	20,000	5000	-
2 to 3	12,000	3500	15,500	500	-
3 to 4	5000	1500	6500	-	8500

Because the load component requires 15 kW of active power, the battery will contribute 10.5 kW, demonstrating why the battery SOC drops from 100% to 99.63% if both sources are present. Otherwise, the coming power will reach 20kW when the irradiation factor and wind speed grow. After feeding the load component, the battery can be charged with the remaining energy. This demonstrates an increase in battery SOC starting at 1.2 s. The provided power from the hybrid generator crosses the 15 kW mark after 1.2 s. The battery SOC will continue to decrease if just the PV or wind systems are used. The battery SOC becomes stable when the wind system starts feeding the load directly and at the maximum supported wind speed, which is 1.5 to 2 s, as illustrated in Figure 8. It is necessary to point out that the battery SOC slope in the wind system is greater than in the PV system. This is owing to the battery's reactive power, which powers the PMSG generator.



(**a**)

Figure 8. *Cont.*

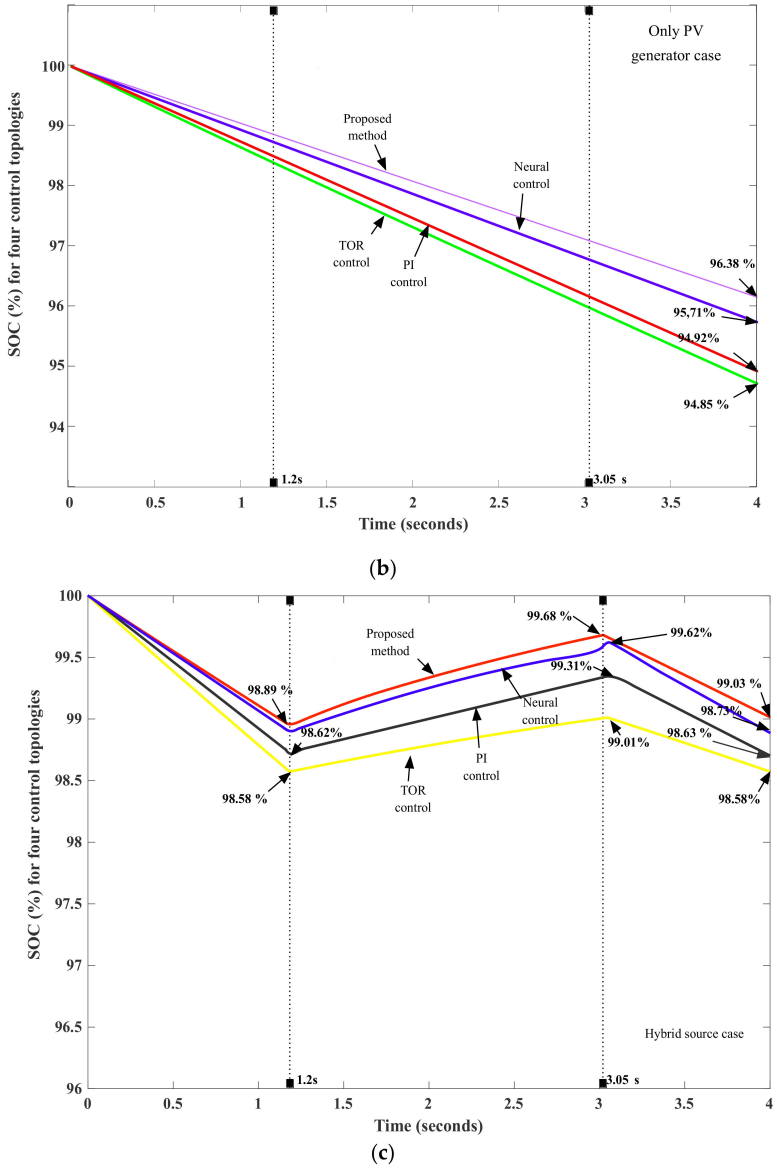


Figure 8. SOC form for three different situations: Case of only wind system is active, Case of only PV generators are valid and the Case of the hybrid energy system in reaction. (**a**) SOC form for four control topologies: cases of only Wind generator case under a constant load. (**b**) SOC form for four control topologies: cases of only PV generator case under a constant load. (**c**) SOC form for four control topologies: cases Hybrid source case under a constant load.

The difference between the four control topologies can be visualized in the various figures in Figure 8. Each source was evaluated by each control method and the hybrid combination was also inspected. The majority of the obtained results show that with the proposed control topology, the battery SOC will be higher than the three other control topologies at the end of the simulation, which proves the benefit of this proposal.

The corresponding duty cycle for each control method such as the relay control, PI control, neural control, and fuzzy control loops are illustrated in Figure 9. It is clear that: the duty cycle evolution is dynamic in the fuzzy control loop, the neural network loop, and with the PI control topology. This proves the situation of the battery charge evolution. However, the duty cycle performance for the relay control loop, illustrated in the same figure, is still constant and was fixed to 75%. Approximately, it is the same situation with the PI control method. However, some perturbation appears when the given power from the hybrid energy source crosses the needed load power. Similar to the fuzzy control

performances, the neural network has a good impact on the given duty cycle form and it touches the maximum value as it is with the fuzzy controller.

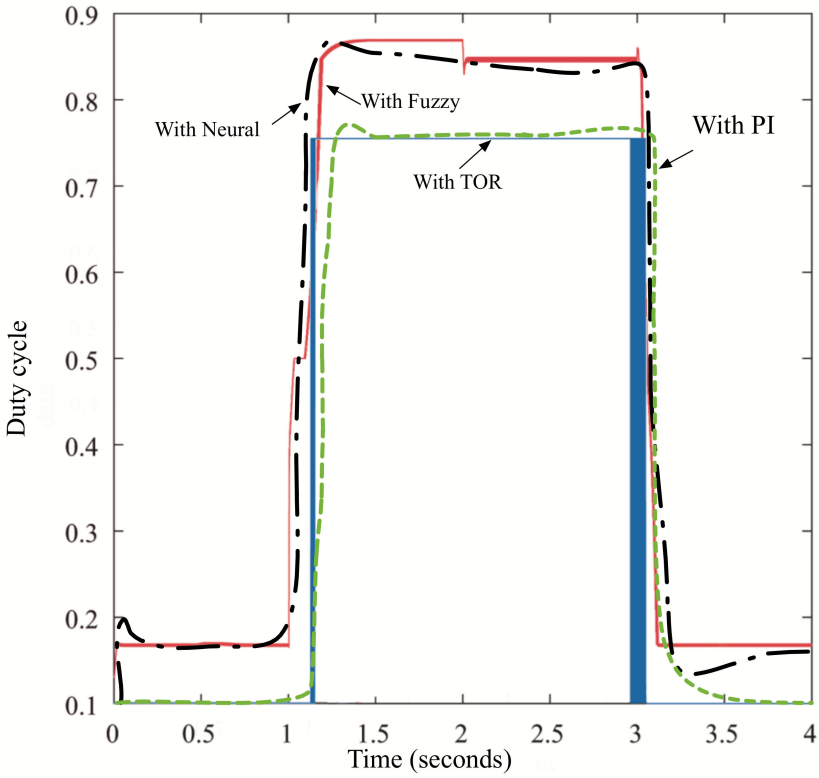


Figure 9. Duty cycle evolution for the four control loops.

Based on the obtained results from the majority of the implemented controllers, such as the relay controller, the neural network controller, the PI controller, and the proposed fuzzy controller, the evolution of the battery state of charge can be regrouped into Table 8. Table 8 shows the SOC trough for 4 s as the simulation time and for constant load comportment. If the hybrid energy source is used, the SOC drops by 0.97% if using the fuzzy controller. However, the SOC will decrease by 1.42% if the relay control technique is used. 1.27% is the difference between the initial and final SOC for the case of the neural controller and 1.37% is the SOC difference if the PI controller is used. Similar to when only one energy source is used, the fuzzy comportment can give an enhanced reaction.

Table 8. A comparison between the SOC losses for the four control methods (case of constant load).

SOC (%) Loss	Only PV Generator	Only Wind Generator	PV and Wind Generators
with fuzzy controller	3.62%	3.35%	0.97%
With neural controller	4.29%	4.00%	1.27%
With PI controller	5.08%	4.82%	1.37%
with Relay controller	5.15%	4.74%	1.42%

Based on these results, the best proposal is related to the fuzzy control loop and the worst solution is related to the relay control method. Therefore, the rest of the comparison will be concentrated on these two specifications and will try to show the benefit of the best control method compared to the worst control loop.

It is necessary to mention that the PI control loop and the neural network control loop can be updated in future endeavors, improving their specific performances and this can improve the global system performance and have a different impact on the power management loop.

So, based on the past specifications of the wind and photovoltaic generators and the preceding battery specifications, it is possible to have a fully recharged battery in 0.46 h using the fuzzy control topology and 1 h using the relay control loop, demonstrating that the fuzzy control loop has a better performance.

4. Application to a Real Case

After applying the fuzzy combination to the overall hybrid prototype, using the MATLAB simulation tool, the obtained results and statistics were generalized for a real case situation. By using real climatic conditions in a specific location in Tunisia, the built application on MATLAB Simulink gave the possible SOC evolution if using the fuzzy or the relay controller. So, the experimental results were obtained by using real climatic conditions and tested on the MATLAB Simulink tool.

In this part, a real case was studied. Based on the statistics given in this study, the application of the power management control approach, which is based on a fuzzy logic controller, can give better global comportment, especially concerning the recharge time. This table gives an estimation of the energy yield for a real case in Djerba island in Tunisia. Figure 10 gives the location of this island and its climatical situation. The statistics try to estimate the possible battery capacity that can be installed in an isolated micro-grid, which feeds 7.5 kW per hour as active power.

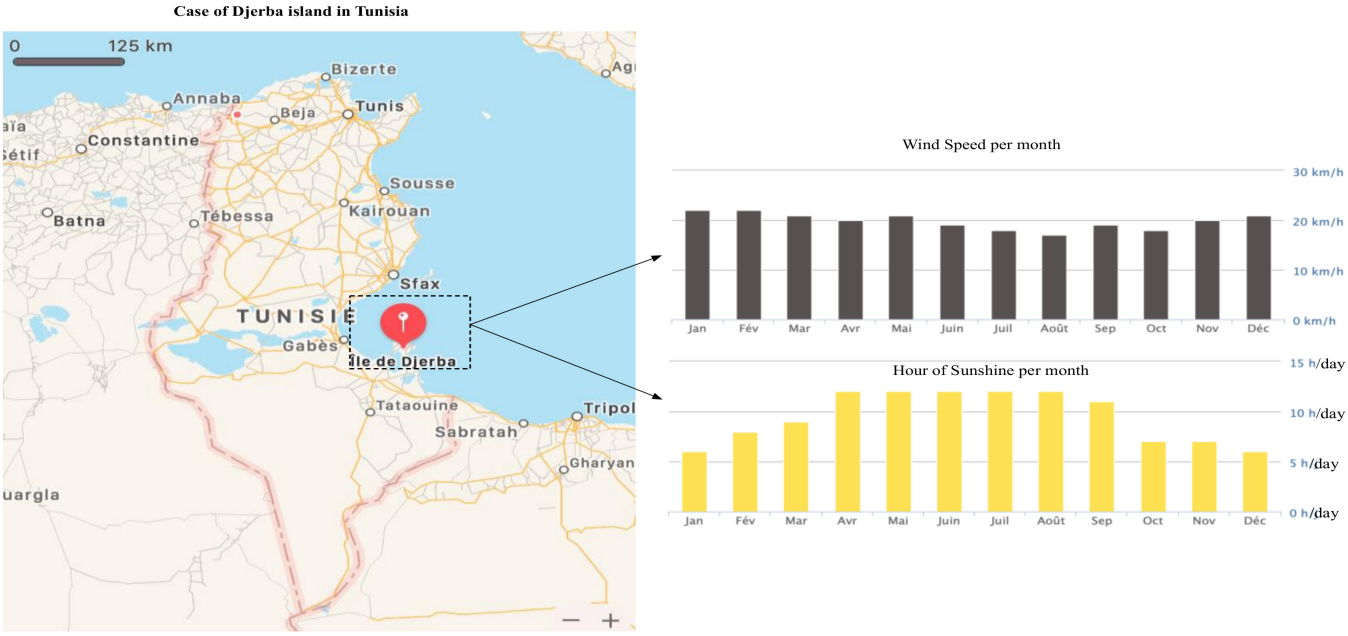


Figure 10. Djerba Island (33°48′ N, 10°51′ E): location and climatic specification.

This study has supposed that at the start of the day, the battery charge is 50%. The results were depicted for the first month of the year in this island location, whose climatic conditions are illustrated in Table 9. For example, in the first month of the year, the solar radiation will be maximum (e.g., 1000 w/m^2) only for one hour per day, and the wind will be existing all day and maximal (e.g., 23 km/h) for 23 h per day. So, the hybrid system will be available with its maximum yield only for one hour per day.

Therefore, the applied test in this section was made only for one day in this month (i.e., January), and the load part was supposed constant at 7.5 kW/h all day.

Table 9. Average hours of solar radiation and wind: the case of Djerba/Tunisia island location.

Month	Jan	Feb	Mar	Apri–Aug
Average Hours of Solar radiation per day	≈ 6 h	≈ 7 h	≈ 8 h	≈ 10 h
Average Hours of Wind per day	≈ 23.50 h	≈ 23.50 h	≈ 23.00 h	≈ 20 h
Average Hours of the maximum of radiation per day	≈ 1 h	≈ 1.5 h	≈ 1.7 h	≈ 2 h
Average Hours of the maximum wind speed per day	≈ 23 h	≈ 23 h	≈ 23 h	≈ 20 h
Month	**Sep**	**Oct–Nov**	**Dec**	
Average Hours of Solar radiation per day	≈ 8 h	≈ 9 h	≈ 6 h	
Average Hours of Wind per day	≈ 20 h	≈ 21 h	≈ 22 h	
Average Hours of the maximum of radiation per day	≈ 11 h	≈ 7 h	≈ 6 h	
Average Hours of the maximum wind speed per day	≈ 16 h	≈ 10 h	≈ 14 h	

Figure 11 shows one battery cell SOC evolution when the hybrid energy system can generate its maximum power, concerning the maximum solar radiation and maximum supported speed of the installed wind system. This is shown in Figure 11, from 1.2 to 2 s.

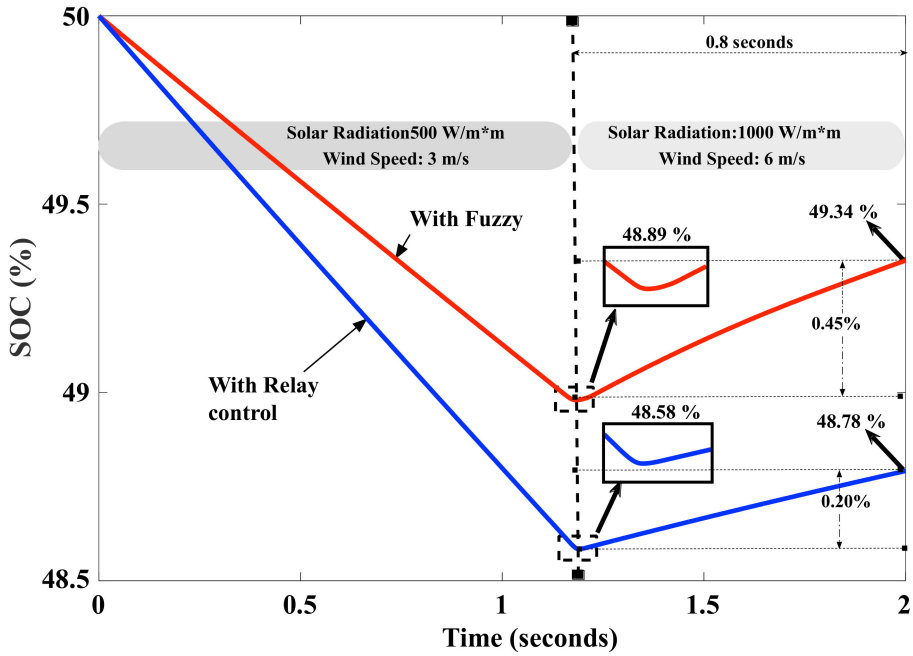


Figure 11. One cell battery SOC evolution, for the studied case in Djerba Island for a constant load demand.

Figure 11 shows two solar radiation and wind speed profiles and gives the state of charge of the battery for each case. As the given power from the hybrid energy system is less than 7.5 kW/h, the battery will participate in feeding the load with the necessary power. So, the battery SOC will decrease. However, it is clear that with the fuzzy logic controller, it is possible to have a gain of 0.31% in 1.2 s.

In the curve of Figure 11, the excess energy will be available for 0.8 s (from 1.2 to 2 s) and this will help charge the battery from 48.58% to 48.78% in 0.8 s if using the relay control and from 48.89% to 49.34% if using the fuzzy controller. It is possible then to conclude that in 0.8 s the battery cell will be charged by 0.20% with the relay control and by 0.45% with the fuzzy controller.

Even, when the hybrid energy system is operating with its maximum capacity, the battery will be then charged by the excess energy given by the source, which is equivalent to 2.54 kW per hour if the fuzzy solution is used and 0.98 kW per hour if the TOR control is implemented. These results were depicted after one hour of simulation time.

Based on the obtained results in Figure 11, it is possible to charge one battery cell having a capacity equivalent to 0.12 kWh, in 176.4 s from 0 to 100% with the fuzzy control method and 440.8 s with the TOR control loop. So, for a battery pack having 6 kWh as battery capacity (The equivalent to 50 cells), it is mandatory to use 8820 s (the equivalent to 2.45 h) for fully charging the battery pack if the fuzzy controller is used. The same method is used for estimating the needed time for fully charging the battery pack with the TOR technique and the needed time is 22,040 s (the equivalent to 6.12 h).

5. Conclusions

The proposed research presents a new control topology for charging a battery pack coupled to an isolated micro-hybrid grid that includes a solar generator, a wind system, and a battery storage system. When the micro-hybrid grid is partially or not operational, the battery pack is linked to feeding the load component. One of the basic objectives of this work is to assure a full recharge situation as rapidly as it is possible. Minimizing the recharge time in such a situation, on the other hand, can help improve battery capacity and provide a bigger power margin for an isolated farm using renewable energy. As a result, the benefits of the suggested control topology have been proven by the provided data and statistics, demonstrating that it is possible to enhance battery capacity by 100% and reduce the recharge time by 50%. The proposed control method was evaluated for four control topologies—the neural network control method, the PI control solution, and the basic relay ON-OFF control loop. It was evaluated for a fixed load demand for various climatic conditions. After proving the benefit of the proposed solution, a statistical analysis was carried out for a real case in Tunisia. For 6 kWh battery capacity, the statistics show that it is possible to fully charge the battery pack in 1.18 h if using the proposed approach, which is 50% of the needed time when the conventional relay ON-OFF controller is used

From the other side, it is important to mention that the real efficiency of this proposed control topology, must be validated for a dynamic load case. This will prove and validate the importance of this solution. Also, as a future endeavor, the optimization of the relay control technique can be a useful solution for the simple control loop and challenging meta-heuristic-based frameworks can be used for that objective. After this optimization, a new comparison for this proposed control loop and the optimized relay control strategy can be used as a perspective for future work.

Author Contributions: All authors contributed equally to this research project. All authors have read and agreed to the published version of the manuscript.

Funding: This research was funded by Ministry of Education in Saudi Arabia under grant number (IF-2020-NBU_406) and by Taif University under grant number (TURSP-2020/277).

Acknowledgments: The authors extend their appreciation to the Deputyship for Research & Innovation, Ministry of Education in Saudi Arabia for funding this research work through the project number (IF-2020-NBU_406). The authors gratefully thank the Prince Faisal bin Khalid bin Sultan Research Chair in Renewable Energy Studies and Applications (PFCRE) at Northern Border University for their support and assistance. Also, the authors thank Taif University for funding this work through the Taif University Research Supporting, Project number (TURSP-2020/277), Taif University, Taif, Saudi Arabia.

Conflicts of Interest: The authors declare no conflict of interest.

List of Symbols

I_{PV}	Total output current	P_{max}	Nominal Maximum Power
I_{Ph}	Current generated by the incident light	V_{max}	Optimum Operating Voltage
I_D	Diode current	I_{max}	Optimum Operating Current
I_P	The current of a parallel resistance	P_w	Wind power
I_0	The diode saturation current	P_m	Mechanical power
I_{sc}	Short circuit current	C_p	Power coefficient of the wind turbine
V_t	Diode thermal voltage	V_v	Wind speed
V_{oc}	Open circuit voltage	λ	Tip speed ratio
R_s	Series resistance	Ω	Rotation speed of the turbine
R_p	Parallel resistance	R	The radius of the rotor blade
K	Boltzmann constant	β	Pitch angle
q	Electron charge	S	The surface of the blade
a	Diode ideality constant	ρ	Air density
K_i	Temperature coefficient of short circuit current	J	Moment of inertia
T	Operating temperature	T_e	Electromagnetic torque
T_n	Nominal temperature	F	Viscosity coefficient of friction
G	Actual sun irradiance	n_s	Number of series cells of a module
G_n	Nominal sun irradiance	P_{PV}	Power PV
E_g	The band gap of silicon at 25°C	V_{PV}	Total output voltage
N_p	Number parallels strings	N_s	Number series strings

References

1. Kayacan, E.; Kayacan, E.; Ramon, H.; Kaynak, O.; Saeys, W. Towards Agrobots: Trajectory Control of an Autonomous Tractor Using Type-2 Fuzzy Logic Controllers. *IEEE/ASME Trans. Mechatron.* **2015**, *20*, 287–298. [CrossRef]
2. Ritzen, P.; Roebroek, E.; Van De Wouw, N.; Jiang, Z.; Nijmeijer, H. Trailer Steering Control of a Tractor–Trailer Robot. *IEEE Trans. Control Syst. Technol.* **2016**, *24*, 1240–1252. [CrossRef]
3. Zhiying, Z.; Haiqing, J.; Shutong, Z.; Jianshe, J. The Electricity Management System of Agricultural Irrigation Based on Fee Control Terminal. In Proceedings of the 2018 China International Conference on Electricity Distribution (CICED), Tianjin, China, 17–19 September 2018; pp. 2–6.
4. AEM. U.S. Tractor and Combine Sales Achieve Positive Results in 2019. Available online: https://www.oemoffhighway.com/market-analysis/industry-news/agriculture/news/21110001/association-of-equipment-manufacturers-aem-us-tractor-and-combine-sales-achieve-positive-results-in-2019 (accessed on 20 September 2021).
5. Tavoosi, J.; Mohammadzadeh, A.; Pahlevanzadeh, B.; Kasmani, M.B.; Band, S.S.; Safdar, R.; Mosavi, A.H. A machine learning approach for active/reactive power control of grid-connected doubly-fed induction generators. *Ain Shams Eng. J.* **2022**, *13*, 101564. [CrossRef]
6. Liu, Z.; Mohammadzadeh, A.; Turabieh, H.; Mafarja, M.; Band, S.S.; Mosavi, A. A New Online Learned Interval Type-3 Fuzzy Control System for Solar Energy Management Systems. *IEEE Access* **2021**, *9*, 10498–10508. [CrossRef]
7. Moayedi, H.; Mosavi, A. Double-Target Based Neural Networks in Predicting Energy Consumption in Residential Buildings. *Energies* **2021**, *14*, 1331. [CrossRef]
8. Band, S.S.; Ardabili, S.; Mosavi, A.; Jun, C.; Khoshkam, H.; Moslehpour, M. Feasibility of soft computing techniques for estimating the long-term mean monthly wind speed. *Energy Rep.* **2022**, *8*, 638–648. [CrossRef]
9. Sahragard, A.; Falaghi, H.; Farhadi, M.; Mosavi, A.; Estebsari, A. Generation Expansion Planning in the Presence of Wind Power Plants Using a Genetic Algorithm Model. *Electronics* **2020**, *9*, 1143. [CrossRef]
10. Panday, A.; Bansal, H. A review of optimal energy management strategies for hybrid electric vehicle. *Int. J. Veh. Technol.* **2014**, *2014*, 160510. [CrossRef]
11. Romero, A.; Carvalho, M.; Millar, D.L. Optimal Design and Control of Wind-Diesel Hybrid Energy Systems for Remote Arctic Mines. *J. Energy Resour. Technol.* **2016**, *138*, 62004–62010. [CrossRef]
12. Maissa, F.; Barambones, O.; Lassad, S.; Fleh, A. A robust MPP tracker based on sliding mode control for a photovoltaic based pumping system. *Int. J. Autom. Comput.* **2017**, *14*, 489–500. [CrossRef]
13. Femia, N.; Petrone, G.; Spagnuolo, G.; Vitelli, M. Optimization of perturb and observe maximum power point tracking method. *IEEE Trans. Power Electron.* **2005**, *20*, 963–973. [CrossRef]
14. Milivojevic, N.; Member, S.; Stamenkovic, I.; Member, S. Electrical Machines and Power Electronic Drives for Wind Turbine Applications. In Proceedings of the 2008 34th Annual Conference of IEEE Industrial Electronics, Orlando, FL, USA, 10–13 November 2008. [CrossRef]

15. Khaligh, A.; Member, S.; Li, Z.; Member, S. Battery, Ultracapacitor, Fuel Cell, and Hybrid Energy Storage Systems for Electric, Hybrid Electric, Fuel Cell, and Plug-In Hybrid Electric Vehicles: State of the Art. *IEEE Trans. Veh. Technol.* **2010**, *59*, 2806–2814. [CrossRef]
16. Wu, F.-B.; Yang, B.; Ye, J.-L. (Eds.) Chapter 4—Operation control technology of energy storage systems. In *Grid-Scale Energy Storage Systems and Applications*; Academic Press: Cambridge, MA, USA, 2019; pp. 83–151. ISBN 978-0-12-815292-8.
17. Nam, S.S.; Alouini, M.; Choi, S. Iterative Relay Scheduling With Hybrid ARQ Under Multiple User Equipment (Type II) Relay Environments. *IEEE Access* **2018**, *6*, 6455–6463. [CrossRef]
18. Rao, L.N.; Gairola, S. PV System Analysis under Partial Shading Using a Sine Model. *Int. J. Renew. Energy Res.* **2018**, *8*, 280–290.
19. Radu, R.; Micheli, D.; Alessandrini, S.; Casula, I.; Radu, B. Modeling and Performance Analysis of an Integrated System: Variable Speed Operated Internal Combustion Engine Combined Heat and Power Unit–Photovoltaic Array. *J. Energy Resour. Technol.* **2015**, *137*, 32001–32010. [CrossRef]
20. Chenouard, R.; El-Sehiemy, R.A. An interval branch and bound global optimization algorithm for parameter estimation of three photovoltaic models. *Energy Convers. Manag.* **2020**, *205*, 112400. [CrossRef]
21. Said, M.; Shaheen, A.M.; Ginidi, A.R.; El-Sehiemy, R.A.; Mahmoud, K.; Lehtonen, M.; Darwish, M.M.F. Estimating Parameters of Photovoltaic Models Using Accurate Turbulent Flow of Water Optimizer. *Processes* **2021**, *9*, 627. [CrossRef]
22. Hammoumi, D.; El Bekkali, C.; Karim, M.; Taoussi, M.; El Ouanjli, N.; Bossoufi, B. Direct controls for wind turbine with PMSG used on the real wind profile of essaouira-Morocco City. *Indones. J. Electr. Eng. Comput. Sci.* **2019**, *16*, 1229–1239. [CrossRef]
23. Angala Parameswari, G.; Habeebullah Sait, H. A comprehensive review of fault ride-through capability of wind turbines with grid-connected doubly fed induction generator. *Int. Trans. Electr. Energy Syst.* **2020**, *30*, e12395. [CrossRef]
24. Asmine, M.; Brochu, J.; Fortmann, J.; Gagnon, R.; Kazachkov, Y.; Langlois, C.-E.; Larose, C.; Muljadi, E.; MacDowell, J.; Pourbeik, P.; et al. Model Validation for Wind Turbine Generator Models. *IEEE Trans. Power Syst.* **2011**, *26*, 1769–1782. [CrossRef]
25. Sørensen, P.; Andresen, B.; Fortmann, J.; Pourbeik, P. Modular structure of wind turbine models in IEC 61400-27-1. In Proceedings of the 2013 IEEE Power & Energy Society General Meeting, Vancouver, BC, Canada, 21–25 July 2013; pp. 1–5.
26. Flah, A.; Irfan, A.K.; Agarwal, A.; Sbita, L.; Marcelo, G. Simoes Field-oriented control strategy for double-stator single-rotor and double-rotor single-stator permanent magnet machine: Design and operation. *Comput. Electr. Eng.* **2021**, *90*, 106953. [CrossRef]
27. Ogunjuyigbe, A.S.O.; Ayodele, T.R.; Adetokun, B.B. Modelling and Analysis of Dual Stator-Winding Induction Machine using Complex Vector Approach Engineering Science and Technology, an International Journal Modelling and analysis of dual stator-winding induction machine using complex vector approach. *Eng. Sci. Technol. Int. J.* **2018**, *21*, 351–363. [CrossRef]
28. Rajan Singaravel, M.M.; Arul Daniel, S. Sizing of hybrid PMSG-PV system for battery charging of electric vehicles. *Front. Energy* **2015**, *9*, 68–74. [CrossRef]
29. Rothenberger, M.J.; Safi, J.; Liu, J.; Anstrom, J.; Brennan, S.; Fathy, H.K. Improving Lithium-Ion Battery Pack Diagnostics by Optimizing the Internal Allocation of Demand Current for Parameter Identifiability. *J. Dyn. Syst. Meas. Control* **2017**, *139*, 081001. [CrossRef]
30. Scrosati, B.; Garche, J. Lithium batteries: Status, prospects and future. *J. Power Sources* **2010**, *195*, 2419–2430. [CrossRef]
31. Di Domenico, D.; Stefanopoulou, A.; Fiengo, G. Lithium-Ion Battery State of Charge and Critical Surface Charge Estimation Using an Electrochemical Model-Based Extended Kalman Filter. *J. Dyn. Syst. Meas. Control* **2010**, *132*, 061302. [CrossRef]
32. El-Sehiemy, R.A.; Hamida, M.A.; Mesbahi, T. Parameter identification and state-of-charge estimation for lithium-polymer battery cells using enhanced sunflower optimization algorithm. *Int. J. Hydrogen Energy* **2020**, *45*, 8833–8842. [CrossRef]
33. Kraiem, H.; Flah, A.; Mohamed, N.; Alowaidi, M.; Bajaj, M.; Mishra, S.; Sharma, N.K.; Sharma, S.K. Increasing Electric Vehicle Autonomy Using a Photovoltaic System Controlled by Particle Swarm Optimization. *IEEE Access* **2021**, *9*, 72040–72054. [CrossRef]
34. Hajia, N.; Venkatesh, B. SOC model of high power Lithium-Ion battery. In Proceedings of the 2015 IEEE Electrical Power and Energy Conference, London, ON, Canada, 24 October 2015; pp. 112–119. [CrossRef]
35. Rezzak, D.; Boudjerda, N. Management and control strategy of a hybrid energy source fuel cell/supercapacitor in electric vehicles. *Int. Trans. Electr. Energy Syst.* **2017**, *27*, e2308. [CrossRef]
36. Tankari, M.A.; Camara, M.B.; Dakyo, B. DC-bus voltage control for multi-sources systems—Battery and Supercapacitors. In Proceedings of the IECON 2011—37th Annual Conference of the IEEE Industrial Electronics Society, Melbourne, VIC, Australia, 7–10 November 2011; pp. 1270–1275. [CrossRef]
37. Reshma Gopi, R.; Sreejith, S. Converter topologies in photovoltaic applications—A review. *Renew. Sustain. Energy Rev.* **2018**, *94*, 1–14. [CrossRef]
38. Patin, N. 2—DC/AC Converters. In *Power Electronics Applied to Industrial Systems and Transports*; Elsevier: Amsterdam, The Netherlands, 2015; Volume 2, pp. 35–100, ISBN 978-1-78548-001-0.